

# EvRT-DETR: The Surprising Effectiveness of DETR-based Detection for Event Cameras

Dmitrii Torbunov<sup>1</sup>, Yihui Ren<sup>1</sup>, Animesh Ghose<sup>1</sup>, Odera Dim<sup>1</sup>, Yonggang Cui<sup>1</sup>

<sup>1</sup>Brookhaven National Laboratory, Upton, NY, USA

dtorbunov@bnl.gov, yren@bnl.gov, aghose@bnl.gov, dodera@bnl.gov, ycui@bnl.gov

## Abstract

*Event-based cameras (EBCs) have emerged as a bio-inspired alternative to traditional cameras, offering advantages in power efficiency, temporal resolution, and high dynamic range. However, the development of image analysis methods for EBCs is challenging due to the sparse and asynchronous nature of the data. This work addresses the problem of object detection for the EBC cameras. The current approaches to EBC object detection focus on constructing complex data representations and rely on specialized architectures. Here, we demonstrate that the combination of a Real-Time DEtection TRansformer, or RT-DETR, a state-of-the-art natural image detector, with a simple image-like representation of the EBC data achieves remarkable performance, surpassing current state-of-the-art results. Specifically, we show that a properly trained RT-DETR model on the EBC data achieves performance comparable to the most advanced EBC object detection methods. Next, we propose a low-rank adaptation (LoRA)-inspired way to augment the RT-DETR model to handle temporal dynamics of the data. The designed EvRT-DETR model outperforms the current, most advanced results on standard benchmark datasets Gen1 (mAP +2.3) and Gen4 (mAP +1.4) while only using standard modules from natural image and video analysis. These results demonstrate that effective EBC object detection can be achieved through careful adaptation of mainstream object detection architectures without requiring specialized architectural engineering. The code is available at: <https://github.com/realtime-intelligence/evrt-detr>.*

## 1. Introduction

Event-based cameras (EBCs) present a biologically inspired alternative to traditional frame-based cameras. Unlike traditional cameras that capture data at a predetermined frame rate, EBC pixels are completely asynchronous and gener-

ate data only when the changes in brightness are detected. This allows the EBCs to have remarkable low power consumption (as low as 10 mW) and reduced data transfer rates. Combined with exceptional temporal resolution (on the order of  $\mu\text{s}$ ) and high dynamic range ( $>100$  dB), EBCs are getting widespread use in various areas, ranging from autonomous driving and robotics to wearable electronics [6].

Despite these advantages, EBC data present unique challenges to computer vision applications. While traditional cameras generate regularly shaped two-dimensional (2D) frames, EBC data are asynchronous streams of pixel events. Each event is a tuple, containing pixel location where the change of brightness occurred, timestamp, and polarity (whether brightness increased or decreased). The events are generated by camera pixels only when the brightness change exceeds a predefined threshold, resulting in data with a high degree of sparsity. The sparse and temporal nature of the EBC data make it nontrivial to directly apply traditional computer vision techniques.

This work addresses the problem of object detection with EBCs. Current solutions to this problem focus on two main directions: (1) constructing sophisticated image-like representations of EBC data (e.g., [34]) and (2) designing novel object detection architectures capable of handling the temporal nature of EBC data (e.g., [20]). Both directions allow for obtaining high-performance object detection methods using EBC data.

While existing EBC object detection methods offer good performance, they come with drawbacks. First, they require extensive engineering effort in both data representation and model architecture design. This creates a specialized development path that diverges from the evolution of object detection methods for frame-based cameras. Such divergence makes it nontrivial to benefit directly from advances in traditional computer vision approaches.

Here, we explore how a state-of-the-art natural image detector, namely the **Real-Time DEtection TRansformer** (RT-DETR) [32], can be effectively adapted to EBCs through a two-stage approach. At the first stage, we use a simple

image-like representation of EBC data and directly train the RT-DETR model on it. Notably, this simple approach already achieves performance comparable to the most advanced EBC-specific object detection methods. This is particularly unexpected as EBC-specific methods attempt to exploit the temporal nature of EBC data and pay attention to the distant past. On the other hand, our method can perform object detection using only a single fixed time window (frame) of  $50ms$ , similar to traditional frame-based cameras.

During the second stage, the RT-DETR model is extended to handle EBC videos, i.e., sequences of fixed time frames. Inspired by efficient adaptation approaches like **Low-Rank Adaptation (LoRA)** [13], we start with our RT-DETR model pre-trained on single frames. We freeze this model and insert a lean recurrent neural networks (RNN)-based temporal processing module in the latent space of its encoder. The designed EvRT-DETR model achieves state-of-the-art performance on the standard benchmark datasets Gen1 [5] and Gen4 [22] using only simple image-like representations of the EBC data and the standard RT-DETR architecture with minimal temporal modifications.

Contributions of this work:

- We demonstrate that RT-DETR, trained on simple image-like representations of EBC data, achieves performance comparable to specialized EBC object detection methods.
- We propose an efficient approach to adapt frozen RT-DETR models for video-based object detection via minimal architectural modifications.
- EvRT-DETR achieves state-of-the-art performance on the standard Gen1 (mAP +2.3) and Gen4 (mAP +1.4) EBC benchmarks using RT-DETR with minimal changes.

## 2. Related Work

Current research on EBC data analysis focuses on two directions. The first is the search for efficient EBC data representations, while the second involves the exploration of neural architectures, best suited for the EBC data.

**Data Representations.** An event camera produces a stream of event data in the form  $(t, p, x, y)$ , where  $t$  is the timestamp of an event,  $p$  is the polarity (positive or negative) of the brightness change, and  $(x, y)$  is the location of the event pixel. To simplify the analysis, the event data often are transformed into alternative representations, more suitable for conventional image analysis algorithms.

The simplest image-like representation of event camera data is known as *Event Frame* or *2D Histogram* representation [6]. To construct this representation, a stream of events from an EBC is partitioned into fixed time windows. Then, events within a time window are accumulated into a 2D frame of the shape  $(2, H, W)$ , where the first dimension

corresponds to an event polarity and the  $(H, W)$  pertain to the index of the camera sensor array.

A natural evolution of the *2D Histogram* representation is a *Stacked 2D Histogram* representation, where each frame is further partitioned into  $T$  fixed time intervals [6]. Such a partitioning results in the data representation of the shape  $(2, T, H, W)$ , which is often reshaped to  $(2T, H, W)$  and treated as a natural image with  $C = 2T$  channels.

The *2D* and *Stacked 2D Histograms* are the simplest and most image-like representations of EBC data. However, directly applying existing computer vision algorithms on such representations results in poor performance [22].

To achieve better performance, other representations are being explored. For example, a *Time Surface (TS)* representation [6, 34] is an image-like representation where pixel values encode the time elapsed since the last event in a given pixel. Thus, unlike the simplest fixed time window representations, TS potentially can encode arbitrarily distant past. Empirically, it has been shown that using the TS representations offers significantly better performance on the object detection tasks compared to the *2D Histogram* representations [22].

Many other EBC data representations also have been proposed. The recent ERGO-12 [34] work has developed efficient image-like representations, achieving state-of-the-art object detection performance on the Gen1 dataset. Meanwhile, other approaches reformulate object detection as a three-dimensional (3D) problem by treating events as points in spatial-temporal space or discretizing them into voxel grids [6]. While computationally heavier, these representations can preserve exact event timing, potentially enabling better handling of overlapping objects and complex motions.

**EBC Object Detection Architectures.** Once the data representation is selected, one can start to develop object detection algorithms. There are several families of object detection methods designed for particular data representations.

For instance, one can use the simplest *2D Histograms* (frames) representation and directly apply conventional image object detection methods on such frames. While being the most straightforward approach, it unfortunately demonstrates relatively poor performance [22].

Several methods built on top of the *2D Histogram* frames extend the analysis to video sequences. Models like Recurrent Vision Transformer (RVT) [10] and State Space Vision Transformer (S5-ViT-B) [35] design neural architectures with various forms of temporal memory to better capture the sequential nature of the EBC frames. Compared to independent frames, using temporal dimension significantly increases the object detection quality.

The most recent family of methods attempts to use more

efficient event representations to further improve the object detection performance. For example, 12-channel Event Representation through Gromov-Wasserstein Optimization (ERGO-12) [34] constructs an optimized image-like event representation and shows that the standard object detection methods perform exceptionally well on it. Alternatively, Asynchronous Spatio-Temporal Memory Network (ASTM-Net) [15] and Adaptive Event Conversion (AEC) [19] attempt to combine both better event representation and use novel neural architectures architecture to expand state-of-the-art results.

Multiple other methods have been developed either treating EBC object detection as a 3D detection problem [9, 22, 26], exploiting benefits of neuromorphic architectures [2], or exploring various hybrid approaches [20, 21].

### 3. Methods

This section describes our approach to the EBC object detection. First, we explain the EBC data representation used, then discuss the structure of the RT-DETR model used as a baseline in our work. Finally, we present the lightweight modifications to the RT-DETR architecture to equip it with video memory.

#### 3.1. Event Representation

As mentioned, we attempt to use a simple pre-processing pipeline and transform EBC data into an image-like *Stacked 2D Histogram* representation [6].

EBCs produce an asynchronous stream of events, where each event is a 4-tuple of the form  $(t, p, x, y)$ . Here,  $t$  is the time stamp of the event,  $p$  is the polarity (positive or negative change of light intensity), and  $(x, y)$  are the spatial coordinates of the pixel that generated a given event. In this work, we partition the stream of events into fixed time windows and buffer the events in each time window into an image-like histogram  $(C, H, W)$  that we refer to as a “frame.”

To ensure direct comparability with existing methods, we adopt the frame construction parameters from RVT [10], which allows us to isolate the impact of our architectural choices from data pre-processing. Specifically, we take the stream of events and partition it into a series of consecutive fixed time windows of  $T_{\text{frame}} = 50$  ms. Each such window corresponds to a single frame. Next, we further subdivide each frame into 10 intervals of  $T_{\text{bin}} = 5$  ms. To construct a frame corresponding to an interval  $[t_0, t_0 + T_{\text{frame}}]$ , we create an intermediate stacked histogram  $S$  from a set of events  $\mathcal{E}$  in that interval:

$$S(p, t_i, y, x) = \sum_{\{e | t_e \in [t_0, t_0 + T_{\text{frame}}]\}} \delta_{x, x_e} \delta_{y, y_e} \delta_{p, p_e} \cdot \mathbf{1}_{[t_i, t_{i+1})}(t_e) \quad (1a)$$

$$t_i = t_0 + i \cdot T_{\text{bin}}, \quad (1b)$$

where  $i \in [0, 10)$  is the bin index,  $(x, y)$  are spatial indices of the event in the EBC matrix, and  $\mathbf{1}$  is an indicator function. Once a stacked histogram  $S$  of shape  $(2, 10, H, W)$  is constructed, we merge the polarity and time dimensions to obtain an image-like 2D frame  $F$  of shape  $(20, H, W)$ .

#### 3.2. The RT-DETR Model

This work relies on the RT-DETR architecture [32] for object detection. The RT-DETR model belongs to a recent family of models spawned by DEtection TRansformer (DETR) [1]. DETR was the first widely successful Transformer-based [29] model developed for object detection. Unlike more traditional convolutional neural network (CNN)-based architectures [11, 25], DETR’s simple and elegant object detection pipeline makes it a compelling alternative.

The DETR model is a hybrid CNN-Transformer model, following a backbone-encoder-decoder architecture. The backbone is a traditional CNN feature extraction backbone (e.g., ResNet [12]), followed by a Transformer encoder transforming the backbone features into tokens and capturing correlations between them. Finally, the decoder part of the DETR is based on a Transformer-decoder architecture. It attempts to decode objects in the image by using cross-attention to the encoder outputs.

The original DETR model has good overall performance [1], but it suffers from significant training instability [30], poor prediction quality for small objects [1], and long inference time [33]. A series of subsequent work [1, 33] has attempted to address these shortcomings by using Feature Pyramid Network (FPN) features, revisiting the role of decoder tokens, and employing deformable attention for efficient feature querying.

Cumulative improvements to the DETR model helped realize the RT-DETR model [32], which exhibits exceptional detection performance for all object scales, stable training, and short inference time. The combination of state-of-the-art performance and real-time inference ( $> 100$ FPS) makes RT-DETR an ideal foundation for EBC object detection.

#### 3.3. Temporal Dependencies

As described in [subsection 3.1](#), we use image-like representations of the EBC data in the form of fixed time frames. While frames can be treated independently, they actually form continuous temporal sequences (videos). The temporal dimension contains valuable information that may help with the object detection problem.

In particular, unlike traditional cameras that capture holistic scenes, EBCs can only detect changes in brightness.

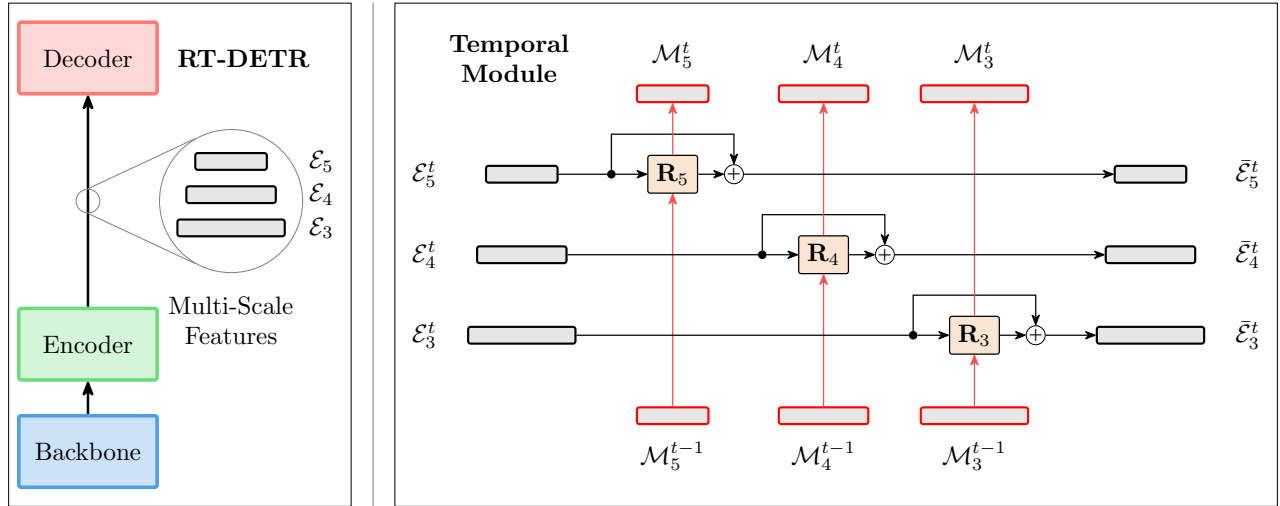


Figure 1. EvRT-DETR backbone and Temporal Module.

In a uniform lighting condition, this is equivalent to being able to detect motion only. A fundamental challenge arises from this property of the EBCs: motionless objects are virtually invisible.

If a motionless object is present in the event camera view, it is still possible to infer its existence indirectly by considering an object’s past history. If at some time in the past the object moved into the camera scene, then its stopping location can be considered a good approximation of the object location at an arbitrary time in the future. Therefore, using object detection architectures with temporal memory may be necessary for the localization of the static objects.

There are multiple ways to approach the problem of designing a memory mechanism for object detection architectures. For instance, recent EBC detection approaches rely on RNN memory mechanisms [10] or on state-space models [35]. On the other hand, natural object detection methods prefer Transformer architectures as a memory mechanism [24].

While both Transformer and RNN architectures potentially can capture temporal dependencies, RNNs have an advantage stemming from an arbitrarily long-range attention span. Having a long-range attention span may be beneficial for tracking stopped objects over long time periods.

Based on these considerations, i.e., long-range attention and implementation simplicity, we adopt an RNN-based memory mechanism in our approach.

### 3.4. EvRT-DETR

Our approach to EBC object detection combines RT-DETR object detection capabilities with an RNN-based temporal memory module, resulting in a hybrid RT-DETR + RNN

architecture, (EvRT-DETR). Then, we train it in a two-stage manner.

At the first stage, we train an RT-DETR model on individual EBC frames (subsection 3.1), treating them as conventional images. This RT-DETR model provides a solid baseline and serves as a foundation for the second stage.

In the second stage, we start with a pre-trained RT-DETR model from the previous stage and freeze it. Next, we equip it with temporal processing capabilities by inserting lightweight RNN modules into the latent space of a frozen encoder. Then, we train only the temporal RNN module on EBC video clips while keeping the baseline RT-DETR frozen.

This modular design has several advantages. First, it clearly separates spatial and temporal feature processing, allowing for a simple swap of different spatial/temporal architectures. Likewise, it allows for using the proven RT-DETR training strategies for the first stage, reducing hyperparameter exploration space. Second, freezing RT-DETR prevents RNN gradient oscillations from destabilizing the base model’s performance. Finally, this separation allows each component to be optimized independently.

#### 3.4.1. Technical Implementation

As shown in Figure 1, our architecture builds on the standard RT-DETR model by adding temporal processing modules to its encoder. In particular, at the end of the RT-DETR encoder, information is represented as a multiscale feature map  $\{\mathcal{E}_3, \mathcal{E}_4, \mathcal{E}_5\}$ , where each pixel corresponds to a Transformer token. For the RT-DETR configurations being considered here, these multiscale features originate from the last three stages of the backbone  $\{\mathcal{S}_3, \mathcal{S}_4, \mathcal{S}_5\}$  [32].

To enable temporal processing, we add three RNN-based

memory modules  $\{\mathbf{R}_3, \mathbf{R}_4, \mathbf{R}_5\}$ . Each RNN module processes its corresponding encoder feature map and updates it via residual connections:

$$(\mathcal{O}_i^t, \mathcal{M}_i^t) = \mathbf{R}_i(\mathcal{E}_i^t, \mathcal{M}_i^{t-1}) \quad (2)$$

$$\mathcal{E}_i^t \rightarrow \mathcal{E}_i^t + \mathcal{O}_i^t, \quad (3)$$

where  $\mathcal{M}_i^t$  is the RNN’s memory for  $i$ -th feature map at time  $t$  and  $\mathcal{O}_i^t$  is the corresponding RNN’s output.

We use the ConvLSTM model [27] as the baseline RNN model because it has proven its efficiency in the RVT model [10].

### 3.5. Data Augmentations

Traditional computer vision methods often emphasize the importance of data augmentation for model generalization [3, 4]. While standard practice when working on natural images, limited research on data augmentations has been done for EBC data [19].

In this work, we treat EBC data as a sequence of image-like frames, enabling the use of standard geometric augmentations. We demonstrate that a simple chain of geometric data augmentations involving random horizontal flip, random rotation, random translation, random scale, and random shear significantly improves object detection performance. Combined with random image patch erasing, it allows our models to achieve state-of-the-art performance.

Augmentation	Magnitude	Probability
Random Horizontal Flip	-	0.5
Random Rotation	$\pm 30^\circ$	0.6
Random Translation	$\pm 0.5$	0.6
Random Scale	(0.5, 1.5)	0.6
Random Shear	$\pm 30^\circ$	0.6
Random Erasure	-	0.4

Table 1. A chain of data augmentations used in this work. Each data augmentation was applied sequentially with the corresponding probability.

Table 1 summarizes a sequence of data augmentations used in this work. We rely on `v2` data augmentations provided by the `torchvision` package (0.17.2) [17]. For the Random Erasure augmentations, we employ the default configuration and deprecated behavior (erasing the image but preserving the corresponding object labels). Each data augmentation in Table 1 is applied independently with a probability  $p$ . If applied, the magnitude of each augmentation is randomly determined within the range specified in the Magnitude column.

**Frame/Video Data Augmentations.** As discussed in subsection 3.4, we train EvRT-DETR in two stages: (1) train

RT-DETR baseline on individual frames and (2) optimize RNN module on video clips.

When training the RT-DETR baseline on individual frames, we apply the data augmentations independently to each frame, following standard computer vision practices. For training the RNN modules on video clips, we modify the data augmentation pipeline by fixing geometric data augmentations (flip, rotation, scale, translation, shear) per video/clip. However, we sample random erasing data augmentation per individual frame. This approach ensures that video frames maintain spatial continuity in temporal dimension and adds a small variation on the per-frame basis.

## 4. Experiments

### 4.1. Datasets

We test our algorithms on two standard EBC object detection benchmarks: *Gen1* [5] and *Gen4* [22] datasets. These datasets have EBC recordings of various driving scenarios collected by Prophesee, a neuromorphic vision technologies company.

**Gen1.** *Gen1* dataset [5] is a widely used automotive dataset for object detection. It contains more than 39 hours of continuous recordings of various driving situations. The dataset was obtained with a GEN1 EBC having spatial resolution of  $304 \times 240$  pixels. For the ease of analysis, the dataset is organized in 60-second video clips and partitioned into train/test splits with 1460 train clips and 470 test clips. *Gen1* is manually annotated at frequencies of  $1 - 4Hz$  (depending on the recording) from a parallel feed of natural image frames. Two classes of objects are annotated: cars and pedestrians.

**Gen4.** *Gen4* [22] (also known as `1MPx`) dataset is collected with a newer GEN4 version of the Prophesee camera. Unlike the GEN1 camera, GEN4 has a larger sensor with a resolution of  $1280 \times 720$ . The *Gen4* dataset features more than 14 hours of driving recordings under various conditions. Similar to *Gen1*, the dataset is split into 60-second video clips and partitioned into train/test splits with 11.19 hours of train videos and 2.25 hours of test videos. The dataset is automatically annotated at 60 Hz frequency. Annotations for cars, two-wheelers, and pedestrians are available for object detection tasks.

### 4.2. Data Pre-processing

We follow the well-established RVT protocols [10] in data pre-processing. We construct event frames as *stacked 2D Histogram* representations of each  $50ms$  time window. Each frame is subdivided into 10 equally time-spaced  $5ms$  intervals. For the *Gen1* dataset with frames of size

Model	Gen1		Gen4		Params (M)
	mAP (%)	FLOPS (G)	mAP (%)	FLOPS (G)	
AsyNet [18]	14.5	-	-	-	11.4
AEGNN [26]	16.3	-	-	-	20.0
Spiking DenseNet [2]	18.9	-	-	-	8.2
Events-RetinaNet [22]	34.0	-	18.0	-	32.8
RED [22]	40.0	16.7	43.0	39.3	24.1
AEC [19]	47.0	20.9	48.4	58.2	46.5
RVT-B [10]	47.2	10.2	47.4	11.9	18.5
GET-T [20]	47.9	16.8	48.4	18.2	21.9
S5-ViT-B [35]	47.4	8.16	47.2	9.57	18.2
ASTMNet [15]	46.7	29.3	48.3	75.7	> 100
SAST-CB [21]	48.2	2.4	48.7	6.4	18.9
ERGO-12 [34]	50.4	69.9	40.6	100.0	59.6
RT-DETR-T (ours)	46.0	7.2	44.1	19.2	20.1
RT-DETR-B (ours)	47.6	15.8	45.2	42.7	42.8
EvRT-DETR-T (ours)	52.3	15.2	49.9	43.3	34.4
EvRT-DETR-B (ours)	<b>52.7</b>	23.9	<b>50.1</b>	66.8	57.1

Table 2. Performance of models on Gen1 and Gen4. Results compiled from [19, 35]

(240, 304), we pad frames by zeros to (256, 320) to ensure divisibility by 32.

For the Gen4 dataset, we downsize images from (720, 1280) to (360, 640) for consistency with previous works. We perform the downsizing by first constructing a full event frame of size (720, 1280) then scaling it down by a factor of 2 with a bilinear interpolation. Similar to the Gen1 dataset, we pad frames by zeros to (384, 640). We slightly deviate from the RVT approach for Gen4, which keeps annotations only for every other frame. Instead, we preserve annotations for all frames because it simplifies data pre-processing and does not produce any visible impact on the model’s performance.

### 4.3. Training

We train EvRT-DETR in two stages. At the first stage, we train the RT-DETR baselines using the Adam optimizer [14]. We use a batch size of 32 and keep the learning rate constant at  $2 \times 10^{-4}$  throughout the training. Following the standard RT-DETR training approach, we keep an exponential moving average (EMA) of model weights with momentum of 0.9999. In total, we train RT-DETR for 400,000 iterations.

For the second EvRT-DETR model training stage, we start with the RT-DETR baseline from the previous step. We freeze the RT-DETR and train an RNN memory module that operates on top of the RT-DETR encoder activations. For the RNN module training, we closely mimic RVT’s setup [10]. Specifically, we train it on a mixture of random and sequential clips of the full videos. For each iteration, we sample 4 random clips and use 4 continuous clips,

giving a total batch size of 8. We reset the memory RNN for each random clip, but we maintain the RNN memory continuity for sequential clips of the same video. For the Gen1 dataset, we use clips of 21 frames and 10 frames for the Gen4 dataset. We rely on the Adam optimizer, 1-cycle learning rate scheduler [28], and a maximum learning rate of  $2 \times 10^{-4}$ . We did not observe any benefit in using EMA for training the RNN memory modules. In total, RNN training runs for 200,000 iterations.

### 4.4. Evaluation Metrics

We evaluate the model performance according to the standard COCO (Common Objects in Context) Mean Average Precision (mAP) measure [16]. For consistency with previous works, we rely on the reference EBC-specific implementation of the COCO metrics provided by Prophesee’s Automotive Dataset Toolbox [22, 23].

### 4.5. Results

Table 2 shows the EvRT-DETR model’s performance compared to results from the literature. For the single-frame training, we present the performance for RT-DETR-T model (RT-DETR PResNet-18 configuration) and RT-DETR-B model (RT-DETR PResNet-50).

As evident from Table 2, directly training the RT-DETR model on the EBC data already affords rather competitive performance without any architecture engineering or data representation design. When augmented by an RNN-plugin, EvRT-DETR outperforms all of the competitors, even in the lightest configuration (EvRT-DETR-T).

In this work, we focus solely on the evaluation of the di-

rect model’s detection performance. While computational efficiency is important, the heterogeneity of reported timing benchmarks in literature (varying hardware configurations, inclusion/exclusion of pre-processing pipelines, numerical precision, graph compilation choices, etc.) makes direct runtime comparisons challenging. Therefore, we present only the model detection performance, leaving systematic and robust timing analysis for future work. Given that the original RT-DETR implementation achieves 108 frames per second (FPS) on natural images of higher resolution than our EBC frames (both Gen1 and Gen4), we expect computational performance to be sufficient for practical applications.

#### 4.6. Ablations

Here, we explore the role of the data augmentations and test our approach with a YOLOX baseline, from the You Only Look Once (YOLO) detector series.

Model	mAP (%)	mAP <sub>50</sub> (%)	mAP <sub>75</sub> (%)
RT-DETR-B (ours)	47.6	76.3	49.5
RT-DETR-B (no augs)	38.6	62.8	39.8
RT-DETR-B (-Rotation)	46.8	74.4	48.8
RT-DETR-B (-Scale)	45.6	73.8	47.2
RT-DETR-B (-Translation)	45.0	72.6	46.2
RT-DETR-B (-Shear)	47.6	75.9	49.7
RT-DETR-B (-Erase)	46.8	75.1	48.7

Table 3. Data Augmentation Ablations on Gen1.

**Data Augmentations.** When the RT-DETR model is trained directly on the benchmark datasets, we observe a significant degree of overfitting and poor model generalizability. Therefore, this work relies heavily on data augmentations.

Table 3 summarizes the ablation study of various data augmentations employed for this effort. The first two rows show the performance of the RT-DETR-B model with and without data augmentations. The subsequent rows demonstrate the model performance changes as we remove one of the data augmentations from the final configuration (the removals are independent not cumulative).

According to Table 3, the RT-DETR-B performance drops by 9 mAP without data augmentations. Among individual contributions, Random Translations and Random Rescaling produce the largest performance gains. Random Rotations and Random Erasing generate comparable but smaller improvement in the model performance. Finally, Random Shear shows minimal impact on the model performance.

**Alternative Baselines.** We have developed an object detection model based on the RT-DETR backbone. A natural question may arise regarding whether the observed im-

Model	mAP (%)	mAP <sub>50</sub> (%)	mAP <sub>75</sub> (%)
RT-DETR-B (ours)	47.6	76.3	49.5
YOLOX-T	36.0	59.9	36.3
YOLOX-S	37.0	61.1	37.6
YOLOX-L	43.1	69.6	44.7
YOLOX-X	43.4	69.7	44.7

Table 4. YoloX on Gen1.

provements are RT-DETR specific or if they can be replicated with other common object detection backbones.

We attempted to replace the RT-DETR baseline by another popular natural image architecture, YOLO, specifically YOLOX [7]. The YOLOX object detection head already has been successfully explored as a part of other EBC object detection architectures [10, 35], making it a natural choice for comparison.

Table 4 demonstrates the performance of the YOLOX object detection baselines on the Gen1 dataset. The YOLOX models are trained using exactly the same setting as the RT-DETR baselines. While the best-performing YOLOX-X model achieves a mAP of 43.4 – lower than RT-DETR-B’s 47.6, it still demonstrates competitive performance compared to specialized EBC architectures. This suggests the effectiveness of natural image detectors on EBC data may extend beyond RT-DETR, particularly to newer iterations of the YOLO family.

## 5. Conclusions

This work demonstrates the surprising effectiveness of the mainstream RT-DETR object detection algorithm for EBCs. We show that RT-DETR applied to basic image-like representations of EBC data achieves performance comparable to specialized EBC-specific methods. Furthermore, our minimal temporal adaptations to the frozen RT-DETR achieve state-of-the-art performance while maintaining architectural simplicity. Additionally, our experiments with YOLOX, while not matching RT-DETR’s performance, suggest the approach of using natural image object detection methods on image-like representations of EBC data may generalize across different architectures. These results indicate that careful adaptation of mainstream detection architectures can be highly effective for EBC data, despite its unique characteristics, potentially reducing the need for specialized architecture development.

## 6. Acknowledgements

This manuscript has been authored by Brookhaven National Laboratory operated by Brookhaven Science Associates, LLC, under Contract Number DE-SC0012704 with the U.S. Department of Energy. The work was funded by the U.S. Department of Energy, National Nuclear Security Admin-

istration, Office of Defense Nuclear Nonproliferation Research and Development.

## References

- [1] Nicolas Carion, Francisco Massa, Gabriel Synnaeve, Nicolas Usunier, Alexander Kirillov, and Sergey Zagoruyko. End-to-end object detection with transformers. In *European conference on computer vision*, pages 213–229. Springer, 2020. 3
- [2] Loïc Cordone, Benoît Miramond, and Philippe Thierion. Object detection with spiking neural networks on automotive event data. In *2022 International Joint Conference on Neural Networks (IJCNN)*, pages 1–8. IEEE, 2022. 3, 6
- [3] Ekin D Cubuk, Barret Zoph, Dandelion Mane, Vijay Vasudevan, and Quoc V Le. Autoaugment: Learning augmentation policies from data. *arXiv preprint arXiv:1805.09501*, 2018. 5
- [4] Ekin D Cubuk, Barret Zoph, Jonathon Shlens, and Quoc V Le. Randaugment: Practical automated data augmentation with a reduced search space. In *Proceedings of the IEEE/CVF conference on computer vision and pattern recognition workshops*, pages 702–703, 2020. 5
- [5] Pierre De Tournemire, Davide Nitti, Etienne Perot, Davide Migliore, and Amos Sironi. A large scale event-based detection dataset for automotive. *arXiv preprint arXiv:2001.08499*, 2020. 2, 5
- [6] Guillermo Gallego, Tobi Delbrück, Garrick Orchard, Chiara Bartolozzi, Brian Taba, Andrea Censi, Stefan Leutenegger, Andrew J Davison, Jörg Conradt, Kostas Daniilidis, et al. Event-based vision: A survey. *IEEE transactions on pattern analysis and machine intelligence*, 44(1):154–180, 2020. 1, 2, 3
- [7] Z Ge. Yolox: Exceeding yolo series in 2021. *arXiv preprint arXiv:2107.08430*, 2021. 7, 10
- [8] Zheng Ge, Songtao Liu, Feng Wang, Zeming Li, and Jian Sun. Yolox is a high-performance anchor-free yolo, exceeding yolov3 v5 with megengine, onnx, tensorrt, ncnn, and opencv supported. <https://github.com/Megvii-BaseDetection/YOLOX>. 10
- [9] Daniel Gehrig and Davide Scaramuzza. Pushing the limits of asynchronous graph-based object detection with event cameras. *arXiv preprint arXiv:2211.12324*, 2022. 3
- [10] Mathias Gehrig and Davide Scaramuzza. Recurrent vision transformers for object detection with event cameras. In *Proceedings of the IEEE/CVF conference on computer vision and pattern recognition*, pages 13884–13893, 2023. 2, 3, 4, 5, 6, 7, 9, 10, 11
- [11] Ross Girshick, Jeff Donahue, Trevor Darrell, and Jitendra Malik. Rich feature hierarchies for accurate object detection and semantic segmentation. In *Proceedings of the IEEE conference on computer vision and pattern recognition*, pages 580–587, 2014. 3
- [12] Kaiming He, Xiangyu Zhang, Shaoqing Ren, and Jian Sun. Deep residual learning for image recognition. In *Proceedings of the IEEE conference on computer vision and pattern recognition*, pages 770–778, 2016. 3
- [13] Edward J Hu, Yelong Shen, Phillip Wallis, Zeyuan Allen-Zhu, Yuanzhi Li, Shean Wang, Lu Wang, and Weizhu Chen. Lora: Low-rank adaptation of large language models. *arXiv preprint arXiv:2106.09685*, 2021. 2, 10
- [14] Diederik P Kingma. Adam: A method for stochastic optimization. *arXiv preprint arXiv:1412.6980*, 2014. 6, 9
- [15] Jianing Li, Jia Li, Lin Zhu, Xijie Xiang, Tiejun Huang, and Yonghong Tian. Asynchronous spatio-temporal memory network for continuous event-based object detection. *IEEE Transactions on Image Processing*, 31:2975–2987, 2022. 3, 6
- [16] Tsung-Yi Lin, Michael Maire, Serge Belongie, James Hays, Pietro Perona, Deva Ramanan, Piotr Dollár, and C Lawrence Zitnick. Microsoft coco: Common objects in context. In *Computer Vision—ECCV 2014: 13th European Conference, Zurich, Switzerland, September 6–12, 2014, Proceedings, Part V 13*, pages 740–755. Springer, 2014. 6
- [17] TorchVision maintainers and contributors. Torchvision: Pytorch’s computer vision library. <https://github.com/pytorch/vision>, 2016. 5
- [18] Nico Messikommer, Daniel Gehrig, Antonio Loquercio, and Davide Scaramuzza. Event-based asynchronous sparse convolutional networks. In *Computer Vision—ECCV 2020: 16th European Conference, Glasgow, UK, August 23–28, 2020, Proceedings, Part VIII 16*, pages 415–431. Springer, 2020. 6
- [19] Yansong Peng, Yueyi Zhang, Peilin Xiao, Xiaoyan Sun, and Feng Wu. Better and faster: Adaptive event conversion for event-based object detection. In *Proceedings of the AAAI Conference on Artificial Intelligence*, pages 2056–2064, 2023. 3, 5, 6, 11
- [20] Yansong Peng, Yueyi Zhang, Zhiwei Xiong, Xiaoyan Sun, and Feng Wu. Get: Group event transformer for event-based vision. In *Proceedings of the IEEE/CVF International Conference on Computer Vision*, pages 6038–6048, 2023. 1, 3, 6
- [21] Yansong Peng, Hebei Li, Yueyi Zhang, Xiaoyan Sun, and Feng Wu. Scene adaptive sparse transformer for event-based object detection. In *Proceedings of the IEEE/CVF Conference on Computer Vision and Pattern Recognition*, pages 16794–16804, 2024. 3, 6
- [22] Etienne Perot, Pierre De Tournemire, Davide Nitti, Jonathan Masci, and Amos Sironi. Learning to detect objects with a 1 megapixel event camera. *Advances in Neural Information Processing Systems*, 33:16639–16652, 2020. 2, 3, 5, 6
- [23] Prophesee. Prophesee’s automotive dataset toolbox. <https://github.com/prophesee-ai/prophesee-automotive-dataset-toolbox>. 6
- [24] Nikhila Ravi, Valentin Gabeur, Yuan-Ting Hu, Ronghang Hu, Chaitanya Ryali, Tengyu Ma, Haitham Khedr, Roman Rädle, Chloe Rolland, Laura Gustafson, et al. Sam 2: Segment anything in images and videos. *arXiv preprint arXiv:2408.00714*, 2024. 4
- [25] J Redmon. You only look once: Unified, real-time object detection. In *Proceedings of the IEEE conference on computer vision and pattern recognition*, 2016. 3
- [26] Simon Schaefer, Daniel Gehrig, and Davide Scaramuzza. Aegnn: Asynchronous event-based graph neural networks. In *Proceedings of the IEEE/CVF conference on computer vi-*

- sion and pattern recognition, pages 12371–12381, 2022. 3, 6
- [27] Xingjian Shi, Zhourong Chen, Hao Wang, Dit-Yan Yeung, Wai-Kin Wong, and Wang-chun Woo. Convolutional lstm network: A machine learning approach for precipitation nowcasting. *Advances in neural information processing systems*, 28, 2015. 5, 9
- [28] Leslie N Smith and Nicholay Topin. Super-convergence: Very fast training of neural networks using large learning rates. In *Artificial intelligence and machine learning for multi-domain operations applications*, pages 369–386. SPIE, 2019. 6, 9
- [29] A Vaswani. Attention is all you need. *Advances in Neural Information Processing Systems*, 2017. 3
- [30] Hao Zhang, Feng Li, Shilong Liu, Lei Zhang, Hang Su, Jun Zhu, Lionel M Ni, and Heung-Yeung Shum. Dino: Detr with improved denoising anchor boxes for end-to-end object detection. *arXiv preprint arXiv:2203.03605*, 2022. 3
- [31] Yian Zhao, Wenyu Lv, Shangliang Xu, Jinman Wei, Guanzhong Wang, Qingqing Dang, Yi Liu, and Jie Chen. Official rt-detr (rtdetr paddle pytorch), real-time detection transformer, detrs beat yolos on real-time object detection. <https://github.com/lyuwenyu/RT-DETR>. 9
- [32] Yian Zhao, Wenyu Lv, Shangliang Xu, Jinman Wei, Guanzhong Wang, Qingqing Dang, Yi Liu, and Jie Chen. Detrs beat yolos on real-time object detection. In *Proceedings of the IEEE/CVF Conference on Computer Vision and Pattern Recognition*, pages 16965–16974, 2024. 1, 3, 4, 9
- [33] Xizhou Zhu, Weijie Su, Lewei Lu, Bin Li, Xiaogang Wang, and Jifeng Dai. Deformable detr: Deformable transformers for end-to-end object detection. *arXiv preprint arXiv:2010.04159*, 2020. 3
- [34] Nikola Zubić, Daniel Gehrig, Mathias Gehrig, and Davide Scaramuzza. From chaos comes order: Ordering event representations for object recognition and detection. In *Proceedings of the IEEE/CVF International Conference on Computer Vision*, pages 12846–12856, 2023. 1, 2, 3, 6
- [35] Nikola Zubic, Mathias Gehrig, and Davide Scaramuzza. State space models for event cameras. In *Proceedings of the IEEE/CVF Conference on Computer Vision and Pattern Recognition*, pages 5819–5828, 2024. 2, 4, 6, 7

## A. Training Setup

In this section, we detail the RT-DETR, EvRT-DETR, and YOLOX configurations used in our experiments.

### A.1. RT-DETR

Our RT-DETR model is based on the reference PyTorch implementation<sup>1</sup> [31, 32]. We explore two RT-DETR configurations: RT-DETR-T (corresponds to RT-DETR-PResNet18) and RT-DETR-B (corresponds to RT-DETR-PResNet50). Our RT-DETR configurations match the reference implementations, except two modifications: (1) we

<sup>1</sup>commit 5b628eaa0a2fc25bdafec7e6148d5296b144af85

change the number of input channels of the backbones from 3 to 20, and (2) we do not use ImageNet pre-trained backbones. Table 5 summarizes the differences between the RT-DETR-PResNet18 and RT-DETR-PResNet50 configurations.

Configuration	RT-DETR-T	RT-DETR-B
Backbone	PResNet-18	PResNet-50
FPN Features	[128, 256, 512]	[512, 1024, 2048]
Encoder Expansion	$\times 0.5$	$\times 1.0$
Decoder Layers	3	6

Table 5. Comparison of the RT-DETR-T and RT-DETR-B Configurations

We train all RT-DETR models for 400,000 iterations using the Adam optimizer [14] with a batch size of 32 and a learning rate of  $2 \times 10^{-4}$ . Similar to the reference RT-DETR training, we maintain an exponential moving average (EMA) of the model weights with a momentum of 0.9999. Unlike the reference RT-DETR training, we do not use any learning rate schedules, nor do we reduce the learning rate of the backbone relative to the encoder-decoder parts.

**Environment.** The RT-DETR training is conducted with PyTorch-2.2.2 and torchvision-0.17.2 on a single NVIDIA RTX A6000 GPU.

### A.2. EvRT-DETR

The EvRT-DETR-T and EvRT-DETR-B models extend RT-DETR-T and RT-DETR-B respectively by adding ConvLSTM modules [27]. Our ConvLSTM blocks use a hidden dimension of 256 (matching the encoder feature maps) and a kernel size of 3 (cf. Appendix B).

The ConvLSTM modules are trained jointly for 200,000 iterations with Adam optimizer and a batch size of 8, while keeping the baseline RT-DETR models frozen. Each batch contains 8 short clips of consecutive frames: 21 frames for Gen1 dataset and 10 frames for Gen4 dataset. The number of frames per clip follows RVT’s approach [10], except we increase the number of frames for the Gen4 dataset from 5 to 10 for better performance. Each batch contains 4 randomly sampled clips and 4 consecutive clips from videos.

Unlike the baseline RT-DETR training with a constant learning rate and EMA averaging, we do not apply EMA averaging to the ConvLSTM modules and use a learning rate scheduler instead. For simplicity, we rely on the RVT-inspired one-cycle LR scheduler [28]. Specifically, we use PyTorch’s OneCycleLR implementation of the scheduler, with the following parameters: maximum LR  $2 \times 10^{-4}$ , initial `div_factor` 20, final `div_factor` 500, `pct_start` 0.0005, annealing strategy “linear”.

The ConvLSTM modules are trained in the same environment as the baseline RT-DETR networks, using a single

NVIDIA RTX A6000 GPU.

### A.3. YOLOX Baselines

We train YOLOX baselines using exactly the same setup as RT-DETR (cf. subsection A.1). We use the reference YOLOX backbone and head implementations<sup>2</sup> [7, 8]. The only modification we implement is changing the number of input channels of the backbone from 3 to 20.

The inference is performed with NMS threshold of 0.65 and confidence threshold of 0.01.

## B. ConvLSTM Ablations

In this section, we examine the design choices of ConvLSTM temporal modules. We investigate the effects of: convolutional kernel size, ConvLSTM block placements, and memory capacity.

Model	mAP (%)	mAP <sub>50</sub> (%)	mAP <sub>75</sub> (%)
EvRT-DETR-B (KS=1)	52.3	81.4	55.4
EvRT-DETR-B (KS=3)	52.7	82.0	56.0
EvRT-DETR-B (KS=5)	52.0	81.3	54.8

Table 6. ConvLSTM Kernel Size vs Performance on Gen1

### B.1. ConvLSTM Kernel Size

Similar to our work, RVT [10] uses ConvLSTM layers to capture the temporal component of EBC data. RVT found that the best performance is achieved with a ConvLSTM kernel size of  $1 \times 1$ . That is, when the ConvLSTM effectively operates as a simple pointwise LSTM.

We replicated RVT’s kernel size exploration for our EvRT-DETR model on the Gen1 dataset. Table 6 shows that, unlike RVT, EvRT-DETR achieves the best performance with a  $3 \times 3$  kernel. However, increasing the kernel size to  $5 \times 5$  degrades performance.

Model	mAP (%)	mAP <sub>50</sub> (%)	mAP <sub>75</sub> (%)
RT-DETR-B (ours)	47.6	76.3	49.5
EvRT-DETR-B [0, 1, 1]	51.0	80.7	54.0
EvRT-DETR-B [1, 0, 1]	52.2	81.3	55.1
EvRT-DETR-B [1, 1, 0]	52.4	81.7	55.3
EvRT-DETR-B [1, 1, 1]	52.7	82.0	56.0

Table 7. ConvLSTM Location vs Performance on Gen1

### B.2. ConvLSTM Location

Our temporal module consists of three ConvLSTM cells – one for each encoder multi-scale feature  $\{\mathcal{E}_3, \mathcal{E}_4, \mathcal{E}_5\}$ . In this subsection we study whether all three ConvLSTM cells are necessary.

<sup>2</sup>commit ac58e0a5e68e57454b7b9ac822aced493b553c53

Table 7 shows the performance degradation observed when one of the cells is removed. The array of 1s and 0s indicates whether the ConvLSTM module is present for each encoder feature  $\{\mathcal{E}_3, \mathcal{E}_4, \mathcal{E}_5\}$ .

The removal of the ConvLSTM cell associated with the lowest multi-scale feature  $\mathcal{E}_3$  leads to significant performance degradation. The removal of  $\mathcal{E}_4$  or  $\mathcal{E}_5$  results in a smaller performance degradation. Table 7 demonstrates that the importance of temporal memory diminishes with increasing feature depth.

Model	mAP (%)	mAP <sub>50</sub> (%)	mAP <sub>75</sub> (%)
EvRT-DETR-B (M=64)	52.1	81.3	54.9
EvRT-DETR-B (M=128)	52.5	81.7	55.6
EvRT-DETR-B (M=256)	52.7	82.0	56.0
EvRT-DETR-B (M=512)	52.9	81.9	56.0

Table 8. ConvLSTM Memory Capacity vs Performance on Gen1

### B.3. ConvLSTM Memory Capacity

For consistency with previous work [10], we use ConvLSTM modules with 256 hidden features. Here, we study the effect of varying this hidden dimension.

Table 8 shows the performance of EvRT-DETR-B with different ConvLSTM hidden dimensions. Since the hidden dimensions of the ConvLSTMs may not match the encoder feature maps  $\{\mathcal{E}_3, \mathcal{E}_4, \mathcal{E}_5\}$ , we use  $1 \times 1$  convolutions to project outputs back to 256 features.

Table 8 indicates that it is possible to reduce the memory capacity of the ConvLSTM modules down to 64 features at a cost of a modest degradation of performance – a mode of operation closely resembling LoRA [13]. The use of 128 or 512 hidden features gives virtually no difference compared to the baseline case of 256.

## C. Gen4-Specific Ablations

In this section we discuss two ablation studies specific to the Gen4 dataset: interpolation mode used for Gen4 downsizing and the effects of changing clip length in ConvLSTM module training.

Model	mAP (%)	mAP <sub>50</sub> (%)	mAP <sub>75</sub> (%)
RT-DETR-B (nearest)	42.3	71.8	42.3
RT-DETR-B (bilinear)	45.2	75.1	46.0
RT-DETR-B (bicubic)	43.1	72.2	43.3

Table 9. Interpolation Method on Gen4

### C.1. Gen4 Resizing and Interpolation

For consistency with previous works, we downscale all Gen4 frames by a factor of 2 from (720, 1280) to (360, 640). We found, however, that RT-DETR performance significantly depends on the interpolation method

used in the downscaling operation. Table 9 compares the performance of the RT-DETR model trained on the Gen4 dataset with different interpolation methods.

Table 9 shows a significant drop in RT-DETR performance when using nearest-neighbor interpolation. Bilinear interpolation gives the best performance, while using bicubic interpolation degrades the results. These results partially overlap with the findings of AEC [19].

Model	mAP (%)	mAP <sub>50</sub> (%)	mAP <sub>75</sub> (%)
EvRT-DETR (5 frames)	49.8	80.7	51.8
EvRT-DETR (10 frames)	50.1	80.9	52.1

Table 10. EvRT-DETR Clip Length Ablation on Gen4

## C.2. Gen4 Clip Length

Our EvRT-DETR training setup for the ConvLSTM module on Gen4 closely follows the RVT setup [10] with one notable exception: the clip length. RVT trains models on clips of 5 frames, while we increase the clip length to 10. Table 10 shows the impact of this change.